



# Electrothermally actuated artificial muscles from the silver-polyethylene-terephthalate core–shell structure

Yu-Lun Liu<sup>1</sup> · Wen-Shin Lee<sup>2</sup> · Fuqian Yang<sup>3</sup> · Hao Ouyang<sup>1</sup> · Sanboh Lee<sup>1</sup> 

Received: 24 June 2022 / Accepted: 10 August 2022 / Published online: 11 August 2022  
© The Polymer Society, Taipei 2022

## Abstract

Developing compliant-artificial muscles for applications in soft robotics and flexible electronics is of practical importance. In this work, we construct Ag-PET (silver-polyethylene-terephthalate) twist-coiled structures from Ag-coated PET. Using electrothermal effect as the actuation mechanism, we demonstrate the contraction of the Ag-PET twist-coiled structures under the action of electric voltage. Increasing electric voltage increases Joule heating, resulting in the increase of the actuation distance and actuation load. Controlling the training load and the rotational speed in the preparation of the Ag-PET twist-coiled structures can tailor the line density of active coils and determine the functionalities of the Ag-PET twist-coiled structures.

**Keywords** Silver coating · Twist-coiled structure · Joule heating · Artificial muscles

## Introduction

The progress in flexible electronics has stimulated the interest in developing compliant-artificial muscles for applications in soft robotics, smart clothes, and smart skins. Among the compliant-artificial muscles, polymer-based materials/structures have been studied under a variety of actuation mechanisms, including electric [1–3], thermal [4–7], and ionic [8–11]. To improve the performance of the compliant-artificial muscles, i.e. high actuation strain and/or high actuation stress, multilayer and core–shell structures have been developed and examined.

Shenoy et al. [12] constructed carbon-coated liquid–crystal elastomer films and demonstrated faster responses to a laser beam due to the increase in heat absorption. Liu et al. [13] prepared a bilayer structure from a compliant film with a multi-wall carbon nanotube/silver nanowire composite and liquid–crystal elastomer and used electrothermal actuation to reach maximum actuation stress

of 0.46 MPa. Yu et al. [14] made core–shell fibers from carbon nanotubes and liquid–crystal elastomer and observed the deflection of the core–shell fibers under light-thermal actuation. Using electroless plating to coat silver (Ag) on the surface of polyethylene-terephthalate (PET), Park et al. [15] prepared an actuator of twisted structure and used Joule heating as the actuation mechanism. Zakeri and Zakeri [16] used soft multilayer actuators to achieve large contraction and expansion. Wang et al. [17] used multiple electrodes to achieve large actuation stress. Currently, few studies are exploring the possibility of using a core–shell structure with a metallic shell and a polymer core to construct compliant-artificial muscles and assess the responses of such artificial muscles solely under the actuation of electric current.

This work is aimed at developing compliant-artificial muscles from an Ag/PET core–shell structure with an Ag shell and a PET core. Electric voltage is used to control the temperature increase of the prepared artificial muscles, in which electric energy is converted to thermal energy through Joule heating, leading to the increase of local temperature. The temperature increase causes the stretch of polymer chains along the extrusion direction and results in the contraction of the artificial muscle.

✉ Sanboh Lee  
sblee@mx.nthu.edu.tw

<sup>1</sup> Department of Materials Science and Engineering, National Tsing Hua University, Hsinchu 300, Taiwan

<sup>2</sup> Department of Athletics, National Taiwan University, Taipei 10617, Taiwan

<sup>3</sup> Department of Chemical and Materials Engineering, University of Kentucky, Lexington, KY 40506, USA

## Experimental details

Monofilament PET fibers of 0.25 mm and 0.48 mm in diameter (YAO I Fabric CO., Ltd, Taiwan) were used in this work. Using the PET fibers, we constructed twist-coiled structures of 28 and 27 cm in length from the PET fibers of 0.48 and 0.25 mm in diameter, respectively. Briefly, PET fibers were grouped and fixed at one end and connected to a DC motor (JD-L003A067, Cheshire Electric Company, LLC, Taiwan) at the other end. Pre-loads of 3.92 and 0.88 N were applied to the PET yarns with the PET fibers of 0.48 and 0.25 mm in diameter, respectively, to limit the self-spinning of the PET fibers before the twist-insertion processing. After the twist-insertion processing, the PET yarns with both ends fixed were placed in an oven at 180 °C for 30 min and then cooled to room temperature in the air to form twist-coiled structures.

Electroless plating was used to coat Ag on the surface of the twist-coiled structures. Briefly, the twist-coiled structures were washed sequentially with acetone, ethanol, and deionized (DI) water for 10 min of each step under ultrasonication. The washed twist-coiled structures were dried at 40 °C for 10 min in an oven and then sensitized at 25 °C for 10 min in an aqueous solution with 10 g/l tin chloride dihydrate and 10 ml/l hydrochloric acids. Using stannous ions ( $\text{Sn}^{2+}$ ) enabled nearly uniform deposition of Ag. Two aqueous solutions were prepared: solution A with silver nitrate 6.8 g/l, ammonium hydroxide, and DI water, and solution B with Rochelle salt 30 g/l, ethanol 20 ml/l, and DI water. The dried twist-coiled structures were placed in the mixture of solution A and solution B, which was maintained at 40 °C for 4 h to allow for the plating of a nearly uniform Ag-film over the twist-coiled structures. After the plating, the Ag-plated twist-coiled structures were washed with DI water and then dried at 40 °C for 10 min in the oven to complete the construction of twist-coiled artificial muscles (TCAMs).

The TCAMs were trained in a furnace under different training loads with the temperature being increased from

room temperature to 85 °C at a heating rate of 3 °C/min and cooled down to room temperature at a rate of 0.5 °C/min. The trained TCAMs were divided into three groups: TCAM-a – training loads of 1.96, 2.94, 3.92, and 4.90 N, rotational speed of 1250 rpm, and PET fiber diameter of 0.48 mm, TCAM-b – training load of 4.90 N, rotational speeds of 1000, 1250, 1500 and 1750 rpm, and PET fiber diameter of 0.48 mm, and TCAM-c – training load of 0.59, 0.88, 1.18 and 1.47 N, rotational speed of 625 rpm, and PET fiber diameter of 0.25 mm.

Optical imaging of the TCAMs was performed on a BX-51 optical microscope (Olympus Optical Co., Japan) equipped with a DFK51AU02 CCD camera (Imaging Source, Germany) under the reflection mode. The morphology of the TCAMs was analyzed on a Scanning Electron Microscope (SEM, JEOL-IT-100, JEOL, Ltd., Japan).

Tensile tests of PET fibers and the TCAMs were conducted on a tensile machine (PT-1996 V, Perfect International Instruments Co., Ltd, Taiwan) at four different cross-head speeds (1, 5, 10, and 50 mm/min). All the tests were done at 25 °C. Electrothermal actuation was performed with a focus on the actuation displacement and the actuation force. For the measurement of the actuation displacement, the TCAMs were subjected to 0.49 and 0.2 N for the PET fibers of 0.48 and 0.25 mm in diameter, respectively. For the measurement of the actuation force, both ends of the TCAMs were clamped under the action of an electric voltage of 2.5, 3, 3.5, or 4 V. The electric current passing through the TCAMs was limited to be less than 0.7 and 0.4 A for the PET fibers of 0.48 and 0.25 mm in diameter, respectively.

Both the electric voltage and current were in-situ measured on a 2450 SourceMeter (Keithley Instruments, USA) using the two-electrode impedance method. The voltage was increased by 0.1 V per 0.5 s. The maximum electric current was set to 1 A to protect the instrument. The temporal evolution of electric current under electric voltage ranging from 2.5 to 4 V was investigated. The maximum electric current was set to 0.95 A to protect the instrument.

**Fig. 1** Optical images of Ag-coated PET coiled fibers of **a** 0.25 mm in diameter and **b** 0.48 mm in diameter

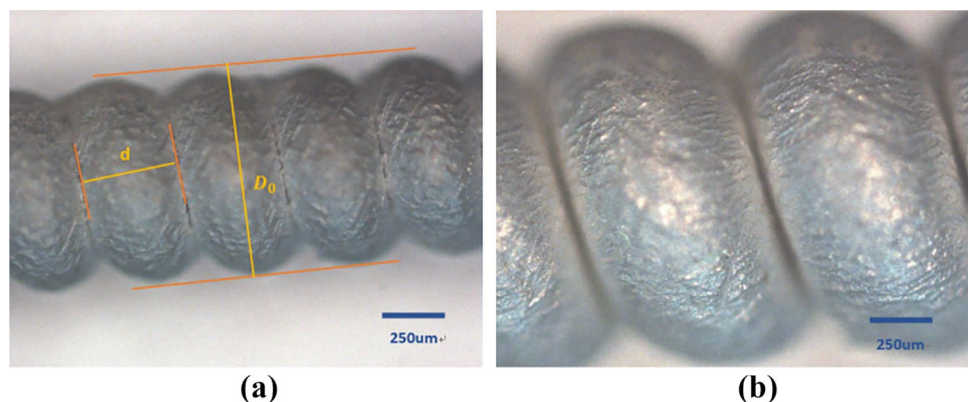
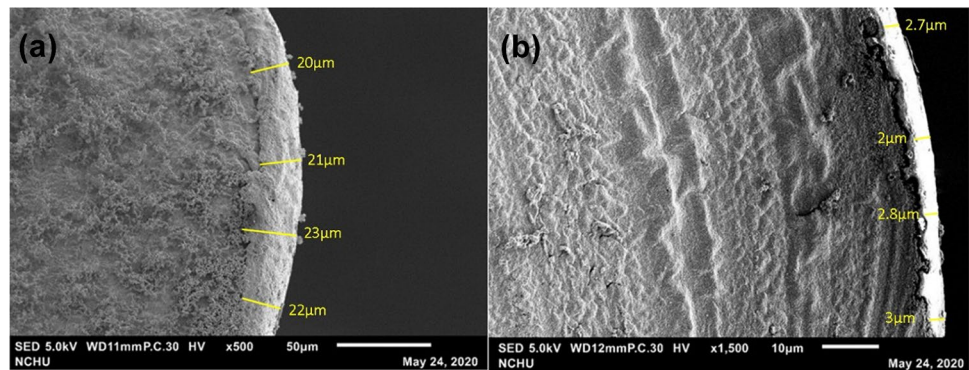


**Fig. 2** SEM images of the cross-section of silver-coated PET fibers of **a** 0.25 mm in diameter and **b** 0.48 mm in diameter



## Results and discussion

Figure 1 shows optical images of Ag-coated PET coiled fibers of 0.25 mm (Fig. 1a) and 0.48 mm (Fig. 1b) in diameter. A layer of Ag is presented on the surface of the PET fibers.

Figure 2 depicts SEM images of the cross-sections of Ag-coated PET fibers of 0.25 mm (Fig. 2a) and 0.48 mm (Fig. 2b) in diameter. There is a distinct outline representing the boundary between the PET core and the Ag shell. Using the SEM images, we estimate the thicknesses of the Ag shells to be  $\sim 21.5$  and  $\sim 2.9$   $\mu\text{m}$  for the PET fibers of 0.25 and 0.48 mm in diameter, respectively.

Using the optical and SEM images, we calculate the geometric dimensions of the TCAMs. Table 1 summarizes the geometric dimensions, training loads and line density of coils (active coils per unit length) of the TCAMs prepared in this work. For the artificial muscles made from the PET fibers of 0.48 mm in diameter except for those made with a rotation speed of 1000 rpm, increasing the rotational speed results in a slight increase of the coil diameter,  $D_0$ , (see Fig. 1a), and the increase of the active coils per unit length for the rotational speed used in this work under the same training load. Note that the artificial muscles made from the PET fibers of 0.48 mm in diameter with a rotation speed of

1000 rpm are unstable. Increasing the training load causes a slight decrease in the active coils per unit length. Such behavior is due to the presence of inelastic deformation of PET fibers, which is irreversible.

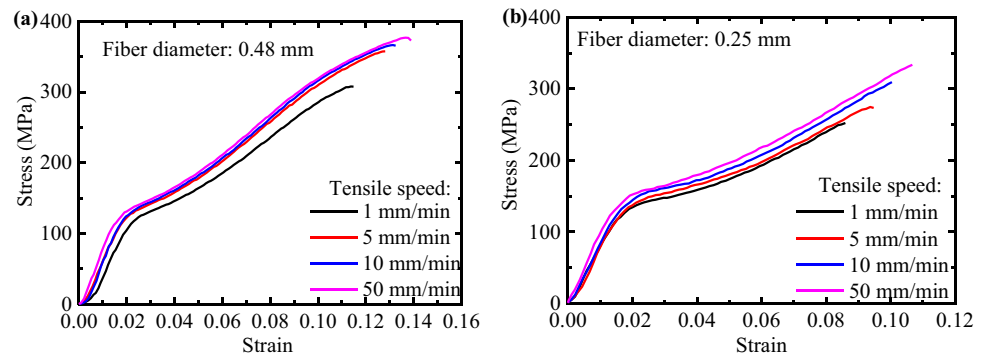
Figure 3 presents engineering stress–strain curves of the Ag-coated PET fibers of 0.48 (Fig. 3a) and 0.25 mm (Fig. 3b) in diameter for primitive fibers under different tensile speeds. The tensile deformation for the Ag-coated PET fibers consists of elastic deformation and plastic deformation with nearly linear hardening. In general, increasing tensile speed increases the strength and yielding point, as expected.

We calculate Young's modulus, yielding stress, and fracture stress of the Ag-coated PET fibers from the engineering stress–strain curves, as listed in Table 2. For reference, the Ag thicknesses are also listed in Table 2. It is evident that increasing the tensile speed increases Young's modulus, yielding stress and fracture strength for respective Ag-coated PET fibers. Such results are consistent with the deformation of PET being controlled by the stretch of polymer chains. Note that Young's modulus and yielding stress of the Ag-PET fibers of 0.48 mm in diameter are smaller than the Ag-PET fibers of 0.25 mm in diameter due to the difference in the thicknesses of the Ag shell, as listed in Table 2.

**Table 1** Geometric dimensions, active coils per unit length ( $N_c$ ), and training load of TCAMs

PET diameter (mm)	Rotation speed (rpm)	$D_0$ (mm)	Training Load (N)	$N_c$ (coils/cm)
0.48	1250	1.15	1.96	$15.2 \pm 0.04$
			2.94	$14.5 \pm 0.06$
			3.92	$14.3 \pm 0.04$
			4.90	$13.4 \pm 0.03$
0.25	625	0.66	0.59	$24.4 \pm 0.14$
			0.88	$22.9 \pm 0.12$
			1.18	$22.4 \pm 0.10$
			1.47	$21.4 \pm 0.09$
0.48	1000	$1.21 \pm 0.03$	4.90	$13.5 \pm 0.04$
			1250	$13.4 \pm 0.03$
			1500	$13.5 \pm 0.03$
			1750	$13.7 \pm 0.04$

**Fig. 3** Stress–strain curves of Ag-coated PET fibers for different tensile speeds: **a** PET fiber of 0.48 mm in diameter, and **b** PET fiber of 0.25 mm in diameter



Figures 4 and S1-2 in Supplementary Information present tensile force–displacement curves of the TCAMs. It is evident that there are two deformation stages – one with linear force–displacement relation, at which the TCAMs can be regarded as a linear spring element with a spring constant,  $K_1$ , and the other with a nonlinear force–displacement relation representing strain hardening associated with the stretch of polymer chains. According to Figs. 4 and S2, the spring constant decreases with the increase of the training load, which can be attributed to the decrease in the line density of active coils (number of coils per unit length). From Fig. S1, we note that the spring constant increases slightly with the increase of the rotational speed for the speed larger than or equal to 1250 rpm under the training load of 4.90 N. This trend can be ascribed to the tightening of the PET fibers at a high rotational speed.

For the nonlinear deformation, we assume that the force and displacement can be expressed as  $F = K\Delta L^n$  with  $F$  as the force,  $\Delta L$  as the displacement,  $K$  as a constant, and  $n$  as the elongation exponent. Using the power-law relationship to fit the curves in Figs. 4 and S1-2, we obtain  $n = 0.7$ ,  $0.7$ , and  $0.8$  for the TCAM-a, TCAM-b, and TCAM-c, respectively. In general, there is no statistical difference between the elongation exponent for all the TCAMs.

Figures 5 and S3-4 in Supplementary Information illustrate the effects of the training load and rotational speed on the actuation distance and actuation force under different applied voltages. It is evident that increasing the training load causes increases in both the actuation distance and

actuation force. Such a trend can be attributed to the increase in the stretch of the polymer chains with increasing the training load without the occurrence of relative slip of polymer chains. According to Fig. S3, both the actuation distance and actuation force increase first with the increase of the rotational speed and then decrease with further increasing the rotational speed. Such behavior implies the occurrence of relative slip of polymer chains under a larger rotational speed, which results in the loss of the actuation capacities.

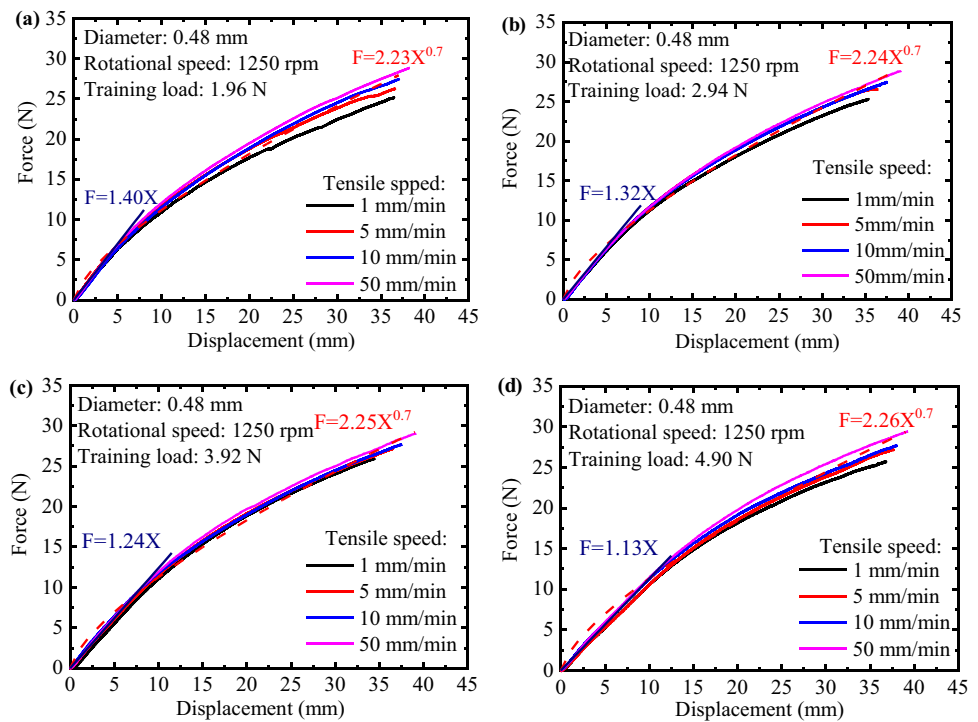
From Figs. 5 and S3-4, we note that both the actuation distance and actuation force increase with the increase of applied voltage. Such behavior is due to the increase of Joule heating with applied voltage. It is known that Joule heat is proportional to the square of electric voltage and inversely proportional to the resistance. Increasing applied voltage leads to the increases of Joule heating and the temperature of the system, which result in the contraction of the TCAMs.

Figure 6 presents I-V curves of TCAMs at a scanning rate of 0.1 V per 0.5 s. All the I-V curves consist of three stages of an initially linear stage for small voltage, a second stage for the rapid increase in electric current, and a third stage for a small increase in electric current to reach a plateau (1 A). Note that the largest current allowed was set to be 1 A in the tests to protect the instrument. The initially linear stage represents the Ohmic behavior with a linear increase of electric current with the applied voltage. From Fig. 6a, c, we note that the slope of the initial linear stage (conductance) decreases with the increase of the training load. The mechanism for such a decrease in conductance is unclear.

**Table 2** Mechanical properties of Ag-coated PET fibers

PET fibers	Ag thickness ( $\mu\text{m}$ )	Tensile speed (mm/min)	1	5	10	50
0.48 mm	2.9	Fracture stress (MPa)	$307.65 \pm 2.82$	$357.67 \pm 3.04$	$365.52 \pm 2.87$	$372.88 \pm 3.31$
		Young's modulus (GPa)	$7.32 \pm 0.09$	$7.59 \pm 0.14$	$8.55 \pm 0.13$	$8.72 \pm 0.16$
		Yield point (MPa)	$98.09 \pm 0.62$	$116.56 \pm 0.83$	$118.87 \pm 0.95$	$127.22 \pm 1.04$
0.25 mm	21.5	Fracture stress (MPa)	$252.29 \pm 1.37$	$273.36 \pm 2.23$	$309.41 \pm 2.68$	$333.62 \pm 3.15$
		Young's modulus (GPa)	$7.71 \pm 0.09$	$8.13 \pm 0.13$	$8.57 \pm 0.16$	$9.08 \pm 0.17$
		Yield point (MPa)	$120.12 \pm 0.73$	$123.01 \pm 0.93$	$132.58 \pm 1.05$	$142.62 \pm 1.12$

**Fig. 4** Force–displacement curves of TCAM-a at different tensile speeds for different training loads of **a** 1.96 N, **b** 2.94 N, **c** 3.92 N, and **d** 4.90 N



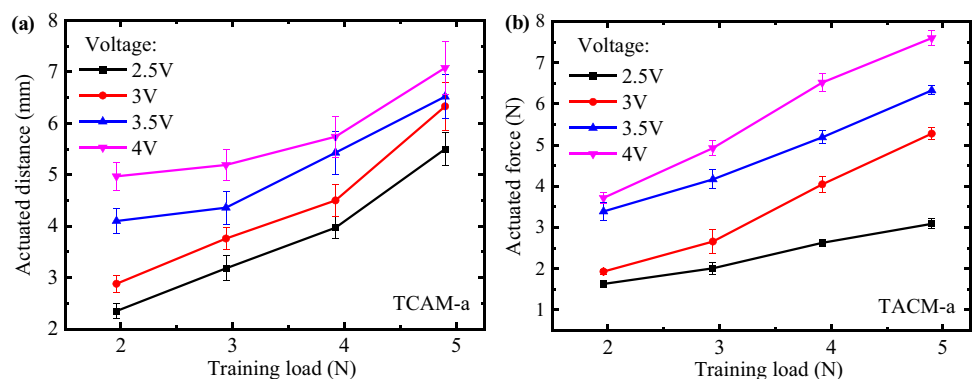
It might be due to the decrease of the line density of active coils, which reduces the cross-sectional area of the TCAMs, leading to the increase in the resistance.

The rapid increase in electric current in the second stage is likely due to the intimate contact between coils due to the large contraction at a large voltage. Further increasing voltage causes an increase in the contact area between coils, leading to a significant decrease in resistance and a significant increase in the current. The plateau behavior in the third stage is due to the limited increase in the contact area between coils after the second stage. This is because of the nonlinear correlation between the contact area and the contact load. There is only a limited increase in the contact area with further increasing the voltage. Note that the plateaus in Fig. 6a, b were due to the limit of 1 A set for electric current to protect the instrument.

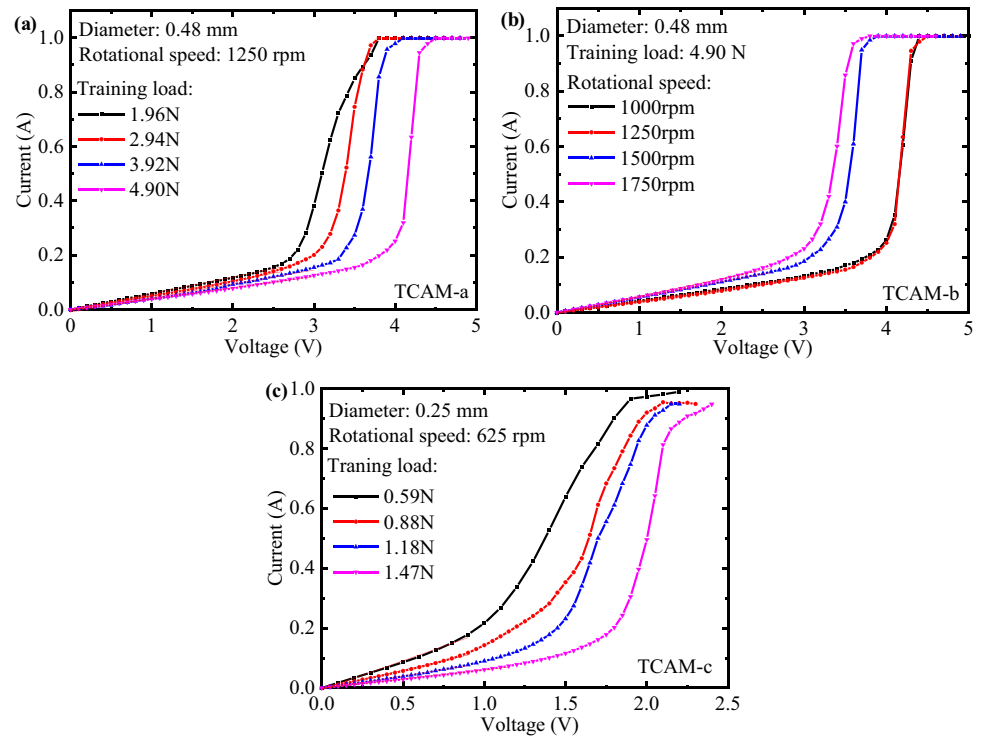
According to Fig. 6b, increasing the rotational speed increases the conductance in the initially linear stage. Such behavior can be attributed to the conductance dependence on the line density of coils. Increasing the rotational speed increases the line density of coils (Table 1), which increases the probability of the contact between coils, leading to an increase in conductance.

To examine if the increase of the electric current is associated with the contraction of TCAMs controlled by Joule heating, we monitored the temporal evolution of the electric current under the action of a constant voltage. Figure 7 presents the temporal evolution of electric current in TCAM-a under different constant voltages for two different training loads of 1.96 (Fig. 7a) and 4.90 N (Fig. 7b). It is evident that applying an electric voltage led to an instantaneous increase of electric current, representing the Ohmic behavior of the

**Fig. 5** Effects of training load on **a** actuation distance and **b** actuation force for TCAM-a



**Fig. 6** I-V curves of TCAMs: **a** TCAM-a, **b** TCAM-b, and **c** TCAM-c. The scanning rate is 0.1 V every 0.5 s

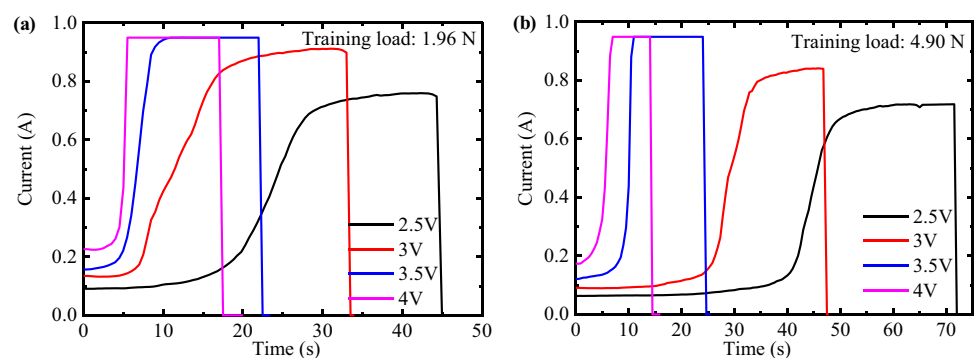


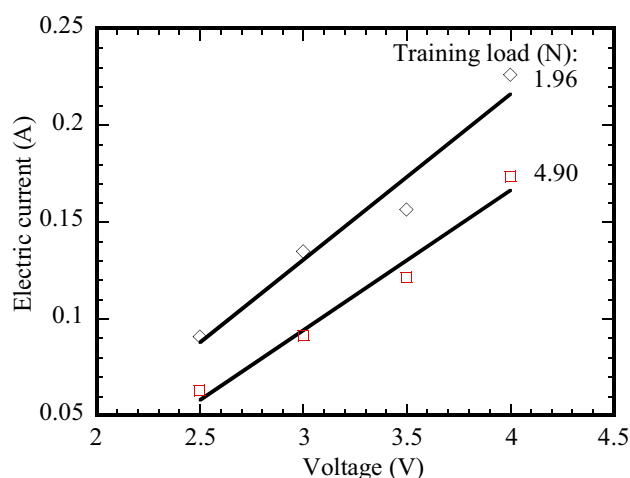
structures. There exists an incubation period, in which the electric current remains approximately unchanged. After the incubation period, the electric current increases rapidly and approaches plateaus eventually. This behavior is attributed to the Joule heating, which causes the contraction of the TCAMs and the contact of the coils, leading to the decrease of the system resistance. After the system reaches a steady state, both the contraction of the TCAMs and the contact of the coils do not change with time and the electric current remains constant afterward. Note that the maximum electric current in Fig. 7 was limited to 0.95 A to protect the instrument.

Figure 8 shows the variation of the instantaneous electric current with electric voltage for the TCAM-a trained by two different training loads of 1.96 and 4.90 N.

The electric current is a linearly increasing function of the electric voltage. Using linear regression to fit the experimental data in Fig. 8, we obtain electric conductance of 0.086 and 0.072  $\Omega^{-1}$  for the TCAM-a trained with the training loads of 1.96 and 4.90 N, respectively. Using Fig. 6a, we obtain electric conductance of 0.061 and 0.041  $\Omega^{-1}$  for the TCAM-a trained with the training loads of 1.96 and 4.90 N, respectively. There exist differences in the electric conductance between the ones calculated in Fig. 8 and the corresponding ones from Fig. 6a, which might be due to the differences in the voltage range. The electric conductance calculated from Fig. 6a is for the electric voltage in a range of 0 to 2.4 V, and the corresponding ones calculated from Fig. 8 are for the electric voltage in a range of 2.5 to 4 V.

**Fig. 7** Temporal evolution of electric current for TCAM-a prepared by two different training loads of **a** 1.96 N and **b** 4.90 N





**Fig. 8** Variation of the instantaneous electric current with an electric voltage of TCAM-a trained with two different training loads of 1.96 and 4.90 N

## Summary

In summary, we have prepared Ag-PET twist-coiled structures, which function as artificial muscles under electrothermal actuation. The principle of electrothermal actuation is the Joule heating associated with the passing of an electric current. The tensile deformation of the Ag-PET twist-coiled structures consists of an initial linear elastic deformation and a nonlinear deformation. The spring constant of the initial linear elastic deformation decreases with the increase of the training load, which can be attributed to the decrease in the line density of active coils (number of coils per unit length). The elongation exponent is in a range of 0.7 to 0.8.

We have studied the electrothermal actuation of the Ag-PET twist-coiled structures and the corresponding current–voltage relation and temporal evolution of electric current under a constant voltage. Increasing the training load increases both the actuation distance and actuation load, and both the actuation distance and actuation load increase first with the increase of the rotational speed and then decrease with further increasing the rotational speed. Both the actuation distance and actuation load increase with the increase of applied voltage due to the increase of Joule heating with applied voltage.

All the current–voltage curves consist of three stages of an initially linear stage for small voltage, a second stage for the rapid increase in electric current, and a third stage for the small increase in electric current to reach plateau. The initially linear stage represents Ohmic behavior with a linear increase of electric current with the applied voltage. The rapid increase of electric current in the second stage is due to the intimate contact between coils associated with the large contraction at a large voltage, and the limited increase in the

contact area between coils after the second stage leads to the plateau behavior in the third stage. The temporal evolution of electric current under a constant voltage further supports the effect of Joule heating on the change of the contact between coils. Increasing the electric voltage shortens the incubation period for the rapid increase of the electric current.

**Supplementary Information** The online version contains supplementary material available at <https://doi.org/10.1007/s10965-022-03233-w>.

**Acknowledgements** SL and HO are grateful to the National Science and Technology Council, Taiwan for their financial support.

## References

1. Bar-Cohen Y (2006) Biomimetics using electroactive polymers (EAP) as artificial muscles - A review. *J Adv Mater* 38:3–9
2. Duduta M, Hajiesmaili E, Zhao H, Wood RJ, Clarke DR (2019) Realizing the potential of dielectric elastomer artificial muscles. *Proc Natl Acad Sci USA* 116:2476–2481
3. Chen YJ, Chen C, Rehman HU, Zheng X, Li H, Liu HZ, Hedenqvist MS (2020) Shape-memory polymeric artificial muscles: Mechanisms, applications and challenges. *Molecules* 25:4246
4. Foroughi J, Spinks GM, Wallace GG, Oh J, Kozlov ME, Fang SL, Mirfakhrai T, Madden JDW, Shin MK, Kim SJ, Baughman RH (2011) Torsional carbon nanotube artificial muscles. *Science* 334:494–497
5. Aziz S, Spinks GM (2020) Torsional artificial muscles. *Mater Horiz* 7:667–693
6. Lee JA, Kim YT, Spinks GM, Suh D, Lepro X, Lima MD, Baughman RH, Kim SJ (2014) All-solid-state carbon nanotube torsional and tensile artificial muscles. *Nano Lett* 14:2664–2669
7. Huang YW, Lee WS, Yang F, Lee S (2019) Tensile deformation of ionic polymer-metal composites: Annealed nylon 6 lines. *Polymer* 177:49–56
8. Shahinpoor M, Bar-Cohen Y, Simpson JO, Smith J (1998) Ionic polymer-metal composites (IPMCs) as biomimetic sensors, actuators and artificial muscles - A review. *Smart Mater Struct* 7:R15–R30
9. Shahinpoor M, Kim KJ (2004) Ionic polymer-metal composites: III. Modeling and simulation as biomimetic sensors, actuators, transducers, and artificial muscles. *Smart Mater Struct* 13:1362–1388
10. He QS, Yin GX, Vokoun D, Shen Q, Lu J, Liu XF, Xu XR, Yu M, Dai ZD (2022) Review on improvement, modeling, and application of ionic polymer metal composite artificial muscle. *J Bionic Eng* 19:279–298
11. Wang YF, Wang F, Kong Y, Wang L, Li QC (2022) Novel ionic bioartificial muscles based on ionically crosslinked multi-walled carbon nanotubes-mediated bacterial cellulose membranes and PEDOT: PSS electrodes. *Smart Mater Struct* 31:025023
12. Shenoy DK, Thomsen DL III, Srinivasan A, Keller P, Ratna BR (2002) Carbon coated liquid crystal elastomer film for artificial muscle applications. *Sens Actuators, A* 96:184–188
13. Liu H, Tian H, Shao J, Wang Z, Li X, Wang C, Chen X (2020) An electrically actuated soft artificial muscle based on a high-performance flexible electrothermal film and liquid-crystal elastomer. *ACS Appl Mater Interfaces* 12:56338–56349
14. Yu Y, Li L, Liu E, Han X, Wang J, Xie Y-X, Lu C (2022) Light-driven core-shell fiber actuator based on carbon nanotubes/liquid crystal elastomer for artificial muscle and phototropic locomotion. *Carbon* 187:97–107

15. Park J, Yoo JW, Seo HW, Lee Y, Suhr J, Moon H, Koo JC, Choi HR, Hunt R, Kim KJ (2017) Electrically controllable twisted-coiled artificial muscle actuators using surface-modified polyester fibers. *Smart Mater Struct* 26:035048
16. Zakeri R, Zakeri R (2022) Bio inspired general artificial muscle using hybrid of mixed electrolysis and fluids chemical reaction (HEFR). *Sci Rep* 12:1–17
17. Wang H, York P, Chen Y, Russo S, Ranzani T, Walsh C, Wood RJ (2021) Biologically inspired electrostatic artificial muscles for insect-sized robots. *Int J Robot Res* 40:895–922

**Publisher's Note** Springer Nature remains neutral with regard to jurisdictional claims in published maps and institutional affiliations.

Springer Nature or its licensor holds exclusive rights to this article under a publishing agreement with the author(s) or other rightsholder(s); author self-archiving of the accepted manuscript version of this article is solely governed by the terms of such publishing agreement and applicable law.